Reports of Practical Oncology and Radiotherapy 25 (2020) 282–292

Available online at www.sciencedirect.com

Reports of Practical Oncology and Radiotherapy

journal homepage: http://www.elsevier.com/locate/rpor

Original research article

A new strategy for craniospinal axis localization and adaptive dosimetric evaluation using cone beam CT

Rafic Kather Hussain Mohamathu, Sujith Christopher, Rajesh Balakrishnan, Babu S Ebenezer Suman, Timothy Peace Balasingh*, Selvamani B, Ravindran Paul B

Department of Radiation Oncology, Christian Medical College, Vellore 632 004, Tamil Nadu, India

ARTICLE INFO

Article history:
Received 16 April 2019
Received in revised form 2 July 2019
Accepted 29 November 2019
Available online 10 December 2019

Keywords:
Craniospinal irradiation
Volumetric modulated arc therapy
Cone beam CT
Adaptive radiotherapy

ABSTRACT

Background and Aim: Computational complexities encountered in craniospinal irradiation (CSI) have been widely investigated with different planning strategies. However, localization of the entire craniospinal axis (CSA) and evaluation of adaptive treatment plans have traditionally been ignored in CSI treatment. In this study, a new strategy for CSI with comprehensive CSA localization and adaptive plan evaluation has been demonstrated using cone beam CT with extended longitudinal field-of-view ($CBCT_{eLFOV}$).

Materials and Methods: Multi-scan CBCT images were acquired with fixed longitudinal table translations (with 1 cm cone-beam overlap) and then fused into a single DICOM-set using the custom software coded in MatLab™. A novel approach for validation of $CBCT_{eLFOV}$ was demonstrated by combined geometry of Catphan-504 and Catphan-604 phantoms. To simulate actual treatment scenarios, at first, the end-to-end workflow of CSI with VMAT was investigated using an anthropomorphic phantom and then applied for two patients (based on random selection).

Results: The fused $CBCT_{eLFOV}$ images were in excellent agreement with planning CT (pCT). The custom developed software effectively manages spatial misalignments arising out of the uncertainties in treatment/setup geometry. Although the structures mapped from pCT to $CBCT_{eLFOV}$ showed minimal variations, a maximum spatial displacement of up to 1.2 cm (and the mean of 0.8 ± 0.3 cm) was recorded in phantom study. Adaptive plan evaluation of patient paradigms showed the likelihood of under-dosing the craniospinal target.

Conclusion: Our protocol serves as a guide for precise localization of entire CSA and to ensure adequate dose to the large and complex targets. It can also be adapted for other complex treatment techniques such as total-marrow-irradiation and total-lymphoid-irradiation.

1. Introduction

Craniospinal irradiation (CSI) plays a vital role in the treatment of medulloblastoma, pineal germ cell tumors and other central nervous system diseases and, rarely, leptomeningeal metastases.[1–3] Traditional CSI planning uses opposing lateral fields for the cranial region and a direct posterior portal for the spinal axis.[3,4] Planning and delivery of CSI is complicated by several factors viz., extensive target length, complex treatment geometry and setup uncertainties.[5] Moreover, the management of the cranial and spinal field junction and beam divergence add to the complexity of the conventional methods.[6] Further, these limitations hinder a favorable clinical outcome in terms of improved local control and reduced normal tissue toxicity. Therefore, an attempt to utilize complex planning techniques such as intensity modulated radiotherapy (IMRT) and volumetric modulated arc therapy (VMAT) for CSI in the pursuit of addressing the above issues while enhancing the dosimetric and clinical benefits is justified. Of the two techniques, the latter is currently considered as the more efficient method in sculpting a highly conformal dose to the craniospinal target.[7,8]

Thus far, several investigators have addressed questions concerning the inverse optimization approach for CSI with various planning strategies.[9–15] Besides, Myers et al. and Lee et al. have described the patient-specific quality assurance (QA) and dosimetric plan verification.[16,17] Modern treatment planning systems (TPS) with large field optimization capabilities enable multi-isocentric

* Corresponding author.
E-mail addresses: raficmphy@gmail.com, raficmphy@cmcvellore.ac.in (K.H.M. Rafic), chrisbon95@gmail.com (C. Sujith), rajeshb@cmcvellore.ac.in (B. Rajesh), emailstoebi@gmail.com (E.S. Babu S), tim_peace@yahoo.co.in (P.B. Timothy), selvamani@cmcvellore.ac.in (B. Selvamani), paul@cmcvellore.ac.in (P.B. Ravindran).

https://doi.org/10.1016/j.rpor.2019.11.003
1507-1367/

VMAT dose calculation for CSI in a single plan. However, the delivery of the same is less forgiving in terms of treatment setup uncertainties[18] due to multiple isocentres and associated field junctions[19] necessitating improved pre-treatment image guidance. Helical Tomotherapy (HT), on the other hand, enables delivery of VMAT in a helical path using continuous synchronized linear movement of the treatment table during the rotatory movement of the gantry which helps avoid abutting field junctions as in the case of the linear accelerator (linac).[20] At present, HT offers equivalent or relatively better dosimetric outcomes for CSI in terms of dose conformity and critical organ sparing as compared to linac-based VMAT.[21] However, the advantage of VMAT over HT is that it requires shorter irradiation time (i.e. fewer monitor units are required to deliver the therapeutic dose) for CSI.[22,23] Such a reduction in irradiation time can have a direct impact on clinical throughput. Moreover, tomotherapy treatment unit is dedicated to specialized techniques and cannot match the versatility of a linac.[24] Consequently, HT is not as available or widely used as VMAT for CSI.

Recently, authors have proposed methods to minimize the errors associated with multiple-field junctions for effective management of CSI with VMAT.[25,26] Madon et al. reported about the image guidance methods for pediatric CSI with individual low-dose cone beam CT (CBCT) protocols for cranial, spinal and posterior fossa irradiation.[27] Although the availability of an integrated CBCT system has led to an improved understanding of treatment/setup uncertainties,[18] the limited longitudinal field-of-view (longi-FOV, 16 cm) has proved to be a hurdle in their potential use for localization of large target volumes encountered in radiotherapy.[28–30] A protocol for extended localization (up to 31 cm longi-FOV) and adaptive dose calculation with CBCT was previously reported by our group for offline image guided adaptive radiotherapy (IGART) of head and neck and pelvic sites.[29,30] However, directly applying this method for CSI encounters complexities due to large craniospinal target and the treatment geometry. To the best of our knowledge, there is no report available on localization of the entire craniospinal axis (CSA) and adaptive treatment planning with CBCT. Therefore, a need arises for formulating a strategy for image guidance and adaptive planning and evaluation for CSI treatment to further reduce the uncertainties related to treatment geometry and patient deformation.

In the present study, we have demonstrated a new strategy for CSI with complete CSA localization and adaptive dosimetric evaluation using CBCT with extended longi-FOV ($CBCT_{eLFOV}$) computed by a custom-developed software. Next, a novel QA approach for comprehensive validation of fused $CBCT_{eLFOV}$ images has been described using combined Catphan phantoms. Finally, the practical usefulness of this strategy, tested and evaluated in a clinical setting using an anthropomorphic phantom and, then, retrospectively applied for two CSI patients treated with VMAT, has been reported.

2. Materials and methods

2.1. Conventional localization protocol

Traditionally, for CSI, two sets of orthogonal kV radiographs or CBCT images are acquired for online rigid registration and locally matched at the superior and inferior centres of the dual-isocentre plan.[16,31] Online image guidance for setup verification and correction is typically scheduled daily for the first three fractions and once weekly thereafter. As per institution protocol, translational (x, y, z) shifts within ±3 mm are acceptable for treatment while systematic errors are corrected in terms of respective couch shifts.

2.2. Proposed CSA localization protocol

According to our protocol, CBCT images were acquired with fixed acquisition parameters viz., 125 kVp, 80 mA and 512 × 512 pixels matrix with 2 mm slice thickness (t). To aid the maximum reconstruction field-of-view (recon-FOV) of 45 cm and an optimum image quality, half-fan (full rotation) acquisition geometry with half bow-tie filter was used as the standard.[29,30] CBCT images were acquired with multiple couch positions with longitudinal translations in steps of fixed increment 'Δ' (= $l - nt$ = 15 cm, where, 'l' is the maximum longi-FOV of standard CBCT and 'n' is the number of slices in the overlap). Based on our findings, 'nt' was optimized to be within 1 cm for all cases to compute the best possible spatial fusion between the identical slices in the overlap. For example, if the slice thickness 't' is 2.5 mm, then the allowed number of slices in the overlap would be limited to 4.

The custom software with a user-friendly graphic user interface (GUI), coded in MatLab™ (vR2018a, The MathWorks Inc, USA), capable of handling up to seven CBCT image sets (each of longi-FOV 15 cm) simultaneously, generates fused $CBCT_{eLFOV}$ images (105 cm longi-FOV). Based on the table top longitudinal position (TTLP, i.e. the absolute 'Z' co-ordinate of the table) extracted from the DICOM header, all the image sets are arranged in a correct sequence. Subsequently, the identical slices in each overlapping region are identified and fused into a single DICOM set after achieving an optimum registration between them using the misalignment management algorithm (MMA). The rigid registration-based MMA script is integrated in the custom software to effectively manage the spatial misalignments arising out of minor differences in treatment setup, couch position and image reconstruction. In all cases, MMA calculates the optimum registration coefficient (μ), as stated in Eq. 1.

$$\mu = \frac{\sum_{j=1}^{n}\sum_{i=1}^{n}\left[\beta\right]_{i,j}}{n^2} \quad (1)$$

where, i, j indicates the rows and columns of the reconstructed CBCT image matrix of order 'n' (i.e. 384 × 384, 512 × 512 or 1024 × 1024 pixels), and $\left[\beta\right]_{i,j} = ([F]_{i,j} - [S]_{i,j})_{identical}$ is the difference in pixel intensity between the identical slices of the first and second image matrices, respectively. The shifts in the vertical and lateral directions correspond to the least 'μ' value.

The central-slices in the abutting region of each series are utilized by the MMA to perform the rigid registration. The 'μ' value is calculated iteratively with a pixel-by-pixel intensity matching of these two central-slices. The least 'μ' value, within a region of interest of 4 mm radius in the vertical and lateral directions, terminates the iteration and the tomographic fusion is executed by applying the corresponding shifts to the remaining slices of the second series and so on. Following this, penumbral HU averaging and local HU correction are performed on the abutting slices and the fused $CBCT_{eLFOV}$ image-set, respectively.[29] The reconstructed blank slices on either side of longi-FOV resulted in case of CBCT acquired with the kV X–ray imaging system (XI) (Fig. 1) in Varian TrueBeam linac will be removed while fusing the overlapping slices.

The fused slices in each overlapping region and the remaining slices of the resultant series are then assigned with same unique identifiers (UID) as that of the first series in order to be imported into the TPS as a single DICOM image-set with extended longi-FOV (i.e. $CBCT_{eLFOV}$) for offline registration and IGART planning of the entire CSA. The reassigned UIDs in the $CBCT_{eLFOV}$ include Frame of Reference, Series Instance, SOP Instance and the Series Number (for image series identification). In addition, a new Instance Number (IN_{new}) to identify each slice in the series and Image Position Patient (IPP) that specifies the x, y, z coordinates of the centre of the first

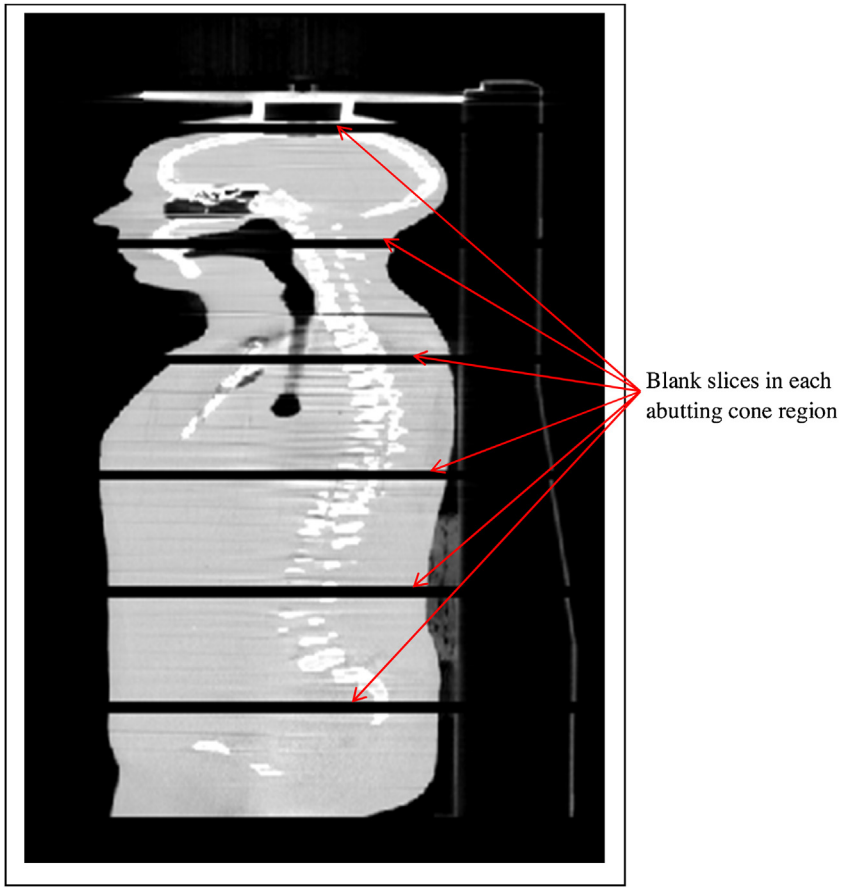

Fig. 1. Reconstructed blank slices in the multi-scanned CBCT image sets (7 half-fan cone beam volumetric scans) of an anthropomorphic phantom with a 1 cm penumbral overlap using the XI system.

voxel transmitted in the image are generated to ensure that the DICOM entities are in continuation with the last slice of the first series as given in the following relationship.

$$IN_{new} = \sum_{i=1}^{m} i + IN_{ref} - \left[\frac{(IN_{ref} + 1)t - \left| Z_{ref} - Z_{\Delta} \right|}{t} \right] \quad (2)$$

where 'm' is the new Instance Number of the last slice in the fused DICOM set, IN_{ref} is the Instance Number of the reference slice (i.e. the last slice) in the first series, Z_{ref} and Z_{Δ} are the TTLP of reference series and the subsequent series with a shift denoted by 'Δ'. The numerical expression in the square brackets of Eq. 2 gives the number of overlapping slices in each abutting region.

2.3. Comprehensive validation of $CBCT_{eLFOV}$

The proposed protocol was extensively evaluated prior to its use for IGART in our clinic. In the present study, a new QA approach of using the Catphan-504 and Catphan-604 (The Phantom Laboratory, USA) phantoms coupled together (as shown in Fig. 2) was demonstrated for validation of fused $CBCT_{eLFOV}$ images. The proposed QA geometry enables a comprehensive set of measurements viz., sensitometry, uniformity, image geometry, high and low contrast sensitivity analysis.

2.4. Protocol robustness evaluation - anthropomorphic phantom study

To test the protocol robustness and to simulate an actual patient treatment, end-to-end (E2E) CSI IGART workflow was investigated. Fig. 3 shows the IGART software interface with fused $CBCT_{eLFOV}$ image of an anthropomorphic phantom setup on-table treatment position. These images were imported to the Eclipse TPS for offline rigid and deformable registrations with the corresponding planning CT (pCT) image set. Subsequently, the structures were mapped onto the $CBCT_{eLFOV}$ and adapted as required. The standard evaluation metrics viz., absolute volume comparison, centre of mass shift ($CMS_{x,y,z}$) and volumetric dice similarity coefficient (DSC_{vol}) of the delineated structures between the pCT and $CBCT_{eLFOV}$, were analyzed. A dosimetric plan comparison was performed to evaluate the deviation from the original dose distribution by superimposing the pCT-based treatment plans onto the HU corrected $CBCT_{eLFOV}$ images. In addition, 3D gamma (γ) evaluation was employed to analyze the variations in high resolution dose distribution computed on the HU-corrected $CBCT_{eLFOV}$ in comparison with reference pCT.

2.5. Clinical evaluation - retrospective patient study

In order to demonstrate the actual clinical scenarios and usefulness of our protocol, the E2E dosimetric analysis of two patients undergoing CSI with VMAT (detailed in the following sections) was included. Unlike the phantom, patients may be subject to inter-fraction anatomical changes and geometric uncertainties. Therefore, to adapt the temporal changes in patient anatomy accurately to the $CBCT_{eLFOV}$, the deformable registration approach was included.

In this study, two distinct data sets were utilized for adaptive CSI plan evaluation: (1) Fused $CBCT_{eLFOV}$ images acquired on table with treated position and (2) Original pCT deformed to $CBCT_{eLFOV}$ (deformed pCT) using modified demons deformable registration

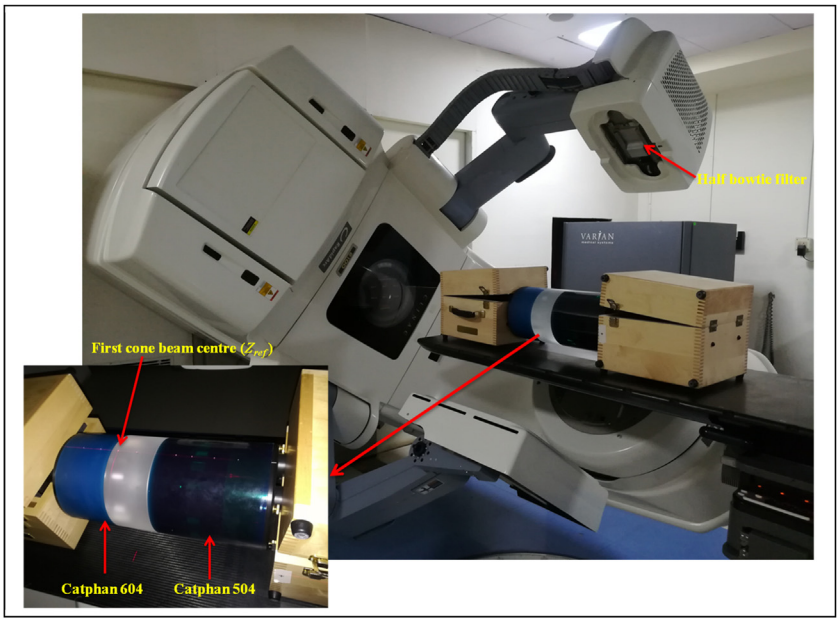

Fig. 2. The acquisition geometry of proposed QA approach using combined Catphan 504 and Catphan 604 phantoms for validation of fused $CBCT_{eLFOV}$ images.

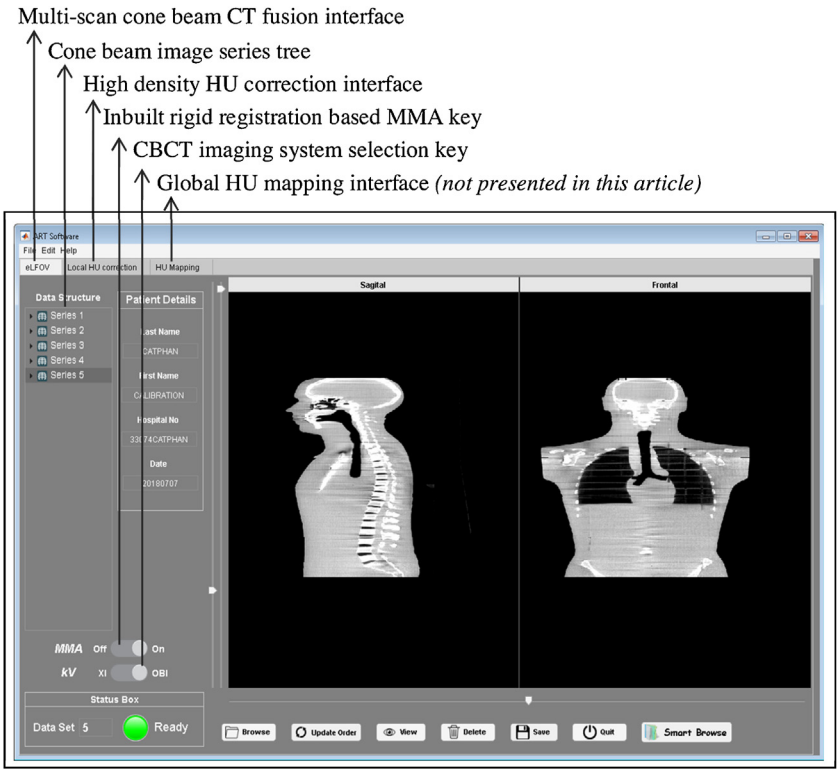

Fig. 3. The custom developed software interface with fused $CBCT_{eLFOV}$ image of an anthropomorphic phantom (fusion of 5 cone beam scans).

algorithm (SmartAdapt, Varian Medical Systems, Palo Alto, CA). Next, the target and OAR structures were carefully evaluated and the redundancies in the deformed original contours were corrected as required prior to mapping them to the $CBCT_{eLFOV}$. At the same time, the deformed initial pCT (source) image sets were assigned the same frame of reference of $CBCT_{eLFOV}$ (target) image sets and imported into the Eclipse TPS. Subsequently, the original treatment plan was mapped onto the $CBCT_{eLFOV}$ as well as deformed pCT image sets and the dose re-calculation procedure was performed. Besides, the same HU values of conventional pCT were employed for dose calculation with deformed pCT; therefore, it was taken as the reference for validating the $CBCT_{eLFOV}$ based adaptive re-plans. Finally, the entire segmentation and dosimetric analysis described in the anthropomorphic phantom study was also investigated for these two patients.

2.6. Patient selection and treatment simulation

Two male patients who were undergoing CSI with VMAT in our institution were randomly chosen for this study. Treatment

simulation was performed in the supine position with hybrid immobilization comprising of thermoplastic mask (Orfit Industries, Wijnegem, Belgium), that immobilizes the patient from head to shoulder and a whole-body Vac-Lok™ (CIVCO Radiotherapy, Orange City, IA) for the rest of the body up to the mid-thigh. The planning CT (pCT) images were acquired (skull to mid-thigh) with 3 mm slice thickness (t) and 512 × 512 pixel resolution with 500 mm reconstruction field-of-view (recon-FOV) using Biograph True Point High Definition CT scanner (Siemens Medical Systems, Germany). As per our protocol, fiducial markers (for CT localization) were defined at two regions, one at the skull base and the other at the T_{12}–L_1 level for treatment guidance.

2.7. Structure delineation and treatment planning

Clinical target volumes including whole brain, spinal canal and the emerging spinal nerve roots and vital organs-at-risk (OARs) viz., eyes, lenses, optic chiasm, brainstem, esophagus, heart, lungs, liver and kidneys, were delineated in the pCT image set using Eclipse TPS (v13.7, Varian Medical Systems, Palo Alto, CA). The cranial and spinal PTVs were created separately by adding a 3 mm symmetric margin for the brain and a 0.5−1 cm asymmetric margin to the spine volumes, respectively. The final PTV was then created by integrating the cranial and spinal PTVs.

Dual-isocentre VMAT treatment plans comprising of four complete arcs (2 arcs/isocentre) with avoidance sectors were computed to deliver a prescription dose of 36 Gy in 20 fractions (180 cGy per day) to the final PTV. For all the cases, X and Y co-ordinates of the isocentres were kept identical so that only longitudinal translation was applied between arcs (superior and inferior) during treatment. In general, the isocentres were placed at C_1– and T_1–vertebrae respectively. As reported by Wang et al., a greater region of overlap of the abutting fields is advantageous in decreasing the maximum dose gradient[1] in CSI treatment plan optimization. In this study, overlaps of 3 cm and 5 cm were used. However, arc geometries, abutting junction and isocentre placements are planner-specific and may also vary depending on the target length. The short summary of the patient demographics, target specification and plan parameters are presented in Table 1. For all the plans (both phantom and patients), pre-treatment patient-specific QA was performed using Octavius1500 array chamber with 4D modular phantom (PTW, Freiburg, Germany) and analyzed with VeriSoft software (v6.2, PTW, Freiburg, Germany).

3. Results

The CSA localization and adaptive dosimetric verification protocol for CSI using custom-developed scripts coded using MatLab yielded clinically acceptable results for both the phantom and the patients. A novel comprehensive approach for validation of the fused slices of Catphan images showed excellent agreement with pCT and standard CBCT. The fused central slices in the two overlapping regions with and without MMA are presented in Fig. 4a. Quantitative evaluations viz., slice geometry, spatial linearity, high and low contrast resolution, spatial uniformity and HU values at high density Teflon insert of $CBCT_{eLFOV}$,were comparable with those of pCT and standard CBCT image sets, summarized in Table 2.

The rigid registration-based MMA effectively handled possible geometric and spatial inaccuracies prior to performing fusion in each overlapping region (Fig. 4b). Table 3 lists and compares the absolute and relative difference in the volume of the target and OARs and their maximum displacement observed in the $CBCT_{eLFOV}$ in comparison with pCT images of an anthropomorphic phantom. The volumes of all the structures delineated on the pCT were found to decrease when mapped onto the $CBCT_{eLFOV}$ with maximum and mean (SD) differences of −1.5% and −0.8% (±0.9%), respectively. Although there was no major difference in the volumes of the mapped structures, a maximum spatial displacement of up to 1.2 cm (with a mean of 0.8 ± 0.3 cm) was recorded in the evaluation. This could be due to a minor rotational shift in treatment setup during online localization as demonstrated in Fig. 5. However, in the case of patients, a non-rigid transformation could also be expected to occur in addition to the changes in treatment geometry. Moreover, the deviations from the original dose distribution, at the spinal PTV regions across the field boundaries when the treatment plan was re-computed onto the $CBCT_{eLFOV}$ of the anthropomorphic phantom, are illustrated in Fig. 6(a and b).

The $CBCT_{eLFOV}$ of one patient acquired during the treatment course with irreproducible hand position is presented in Fig. 7. Variation in vital structures mapped from pCT onto the $CBCT_{eLFOV}$ through rigid and deformable registrations, updated independently on both $CBCT_{eLFOV}$ and deformed pCT image sets by the same physician, was found to have similar tendency. The mean variation in $CMS_{x,y,z}$ and DSC_{vol} metrics in comparison with initial pCT is summarized in Table 4. Specific conclusions on the importance of these metrics in terms of dosimetric end points could not be made due to the limited number of clinical examples included in this study. However, a consistent pattern of $CMS_{x,y,z}$ results was observed between the pCT and $CBCT_{eLFOV}$ as well as pCT and deformed pCT images (of both the phantom and the patients), except for the eyes and cranial PTV structures of one patient, with the mean maximum lateral shift (x-axis) of 1.5 ± 0.2 cm.

As there is no influence of anatomical and treatment related uncertainties in the contour propagation, superior DSC_{vol} results with lower SD (0.97 ± 0.02) were recorded for the anthropomorphic phantom. Similarly, consistent but lower DSC values viz., 0.74 ± 22 and 0.70 ± 0.28, than the desirable results (0.95), were observed for the patients. These results suggest that even small unaccounted uncertainties during CSI treatment may have a larger impact on the contour mapping and dosimetric outcome. Table 5 summarizes the 3D γ-evaluation results of CSI VMAT plans when re-computed on the adaptive $CBCT_{eLFOV}$ and deformed pCT image sets of both anthropomorphic phantom and the patient study.

4. Discussion

In the present study, we have successfully demonstrated the comprehensive localization and adaptive dosimetric evaluation strategies for CSI within the planned course of treatment. Also, we have showed a simplified protocol, not restricted to CSI, ensures precise delivery of prescribed dose to the large target volumes without the need for increased PTV margins. Integrating this method in the online pre-treatment imaging protocols and the treatment console of modern linac would help ensure adequate dose to the target.

A new QA strategy proposed in our study by combining Catphan-504 and Catphan-604 phantoms was found to be an efficient method to test the robustness of CSA localization protocol. With this simple and reproducible QA approach, one can validate the spatial linearity, contrast resolution and HU accuracy of fused slices of $CBCT_{eLFOV}$ image sets simultaneously. The QA strategy proposed above can also be performed by combining other models of Catphan phantoms, however, a thorough knowledge of the phantom geometries is required while performing the analysis.

Our results confirmed the need for standardization of large treatment volume localization and adaptive dosimetric evaluation for precise delivery of prescribed dose to the target. One of the key findings in our study was that even small rotational shifts at the isocentre level could lead to a gross shift in dose delivered to (the

Table 1
Patient and plan demographics.

Study	Age (years)	Sex	Final PTV		Inferior isocentre co-ordinates (x, y, z) relative to superior isocentre (cm)	Abutting field overlap (cm)	Total monitor units (MU)
			Length (cm)	Volume (cc)			
Anthropomorphic Phantom	–	Male	69.3	1155.8	0, 0, 31	1	780
Patient 1	9	Male	53.7	2017.2	0, 0, 30	1.5	772
Patient 2	10	Male	58.3	2578.6	0, 0, 30	5	889

Table 2
Comprehensive evaluation of multi-scan $CBCT_{eLFOV}$ image quality and HU value with proposed QA strategy.

Scan (imaging parameters)	High contrast resolution (No. of line pairs)		Low contrast resolution (No. of circles)		Spatial linearity, cm (x, y)		Spatial uniformity (HU)		Circular symmetry, cm (x, y)		Slice geometry at centre fusion, cm (x, y)		Hounsfield unit at Teflon inserts	
	CTP 604	CTP 504	CTP 604	CTP 504	CTP 604	CTP 504	CTP 604	CTP 504	CTP 604	CTP 504	CTP 604	CTP 504	CTP 604	CTP 504
pCT (110 kVp, 200 mA)	4	5	6	8	5.01, 5.01	5.01, 5.00	9	10	20.0, 20.0	20.0, 20.0	1.97, 1.97	2.00, 2.02	935	932
Standard CBCT (125 kVp, 80 mA)	4	5	5	5	4.96, 4.96	4.96, 5.00	−19	−28	19.8, 19.8	19.9, 19.9	1.97, 1.97	2.02, 2.02	964	941
Proposed $CBCT_{eLFOV}$ (125 kVp, 80 mA)	4	5	5	5	4.92, 4.92	4.92, 4.92	−17	−31	19.9, 19.9	19.9, 19.9	2.00, 2.00	2.00, 2.00	994	973

Table 3
Evaluation of mapped structures through rigid registration (Anthropomorphic phantom study).

Structures	Absolute volume (cc)		Difference		Maximum displacement (cm)
	pCT	$CBCT_{eLFOV}$	Absolute (cc)	Relative (%)	
Cranial PTV	1155.8	1147	8.8	0.8	1.2
Spinal PTV	207.3	201.2	6.1	2.9	0.8
Brainstem	25.4	25.3	0.1	0.4	0.5
Eye left	6.8	6.7	0.1	1.5	0.5
Eye right	6.7	6.6	0.1	1.5	0.5
Lung left	1669.8	1664.6	5.2	0.3	1.2
Lung right	1982.5	1977.9	4.6	0.2	0.9
Kidney left	47.1	46.9	0.2	0.4	0.9
Kidney right	47.1	46.8	0.3	0.6	1.0
Liver	303.4	303.4	0.0	0.0	0.8
Heart	520.7	522.1	−1.4	−0.3	0.5

Table 4
Mean (range) $CMS_{x,y,z}$ and DSC_{vol} comparisons of evaluated structures.

Image sets	pCT vs. $CBCT_{eLFOV}$	pCT vs. deformed pCT	Deformed pCT vs. $CBCT_{eLFOV}$
	Centre of mass shift (X, Y, Z) in mm		
Rando	0 (0–0.3), 0.4 (0–3.0), 0.6 (0.1–1.8)	–	–
Patient 1	0.7 (0–4.9), 0.7 (0.1–4.2), 1.4 (0.1–6.6)	0.7 (0–4.8), 0.7 (0–4.2), 1.5 (0.0 - 6.8)	0 (0–0.2), 0 (0–0.2), 0.2 (0.1 - 0.6)
Patient 2	4.2 (0.5–16.9), 0.3 (0–2.5), 0.3 (0.1–6.5)	4.2 (0.2–16.9), 0.3 (0–2.4), 0.5 (0.2–6.4)	0 (0–0.1), 0 (0–0.1), 0.2 (0–0.8)
	Volumetric dice similarity co-efficient		
Rando	0.97 (0.92–1.00)	–	–
Patient 1	0.74 (0.29–0.97)	0.76 (0.35–0.99)	0.94 (0.82–0.98)
Patient 2	0.70 (0.12–0.90)	0.70 (0.12–0.90)	0.93 (0.78–0.98)

Table 5
3D gamma evaluation results.

Study	2% DD/2 mm DTA		3% DD/3 mm DTA	
	pCT vs. $CBCT_{eLFOV}$			
	Global	Local	Global	Local
Rando	98.3	88.7	99.2	96.5
Patient 1	91.5	80.0	94.2	90.6
Patient 2	93.2	85.8	96.0	92.9
	pCT vs. deformed pCT			
Rando	–			
Patient 1	91.2	86.1	93.9	92.1
Patient 2	92.8	88.5	95.7	93.8
	$CBCT_{eLFOV}$ vs. deformed pCT			
Rando	–			
Patient 1	98.8	96.4	99.6	99.1
Patient 2	99.7	96.8	100.0	99.0

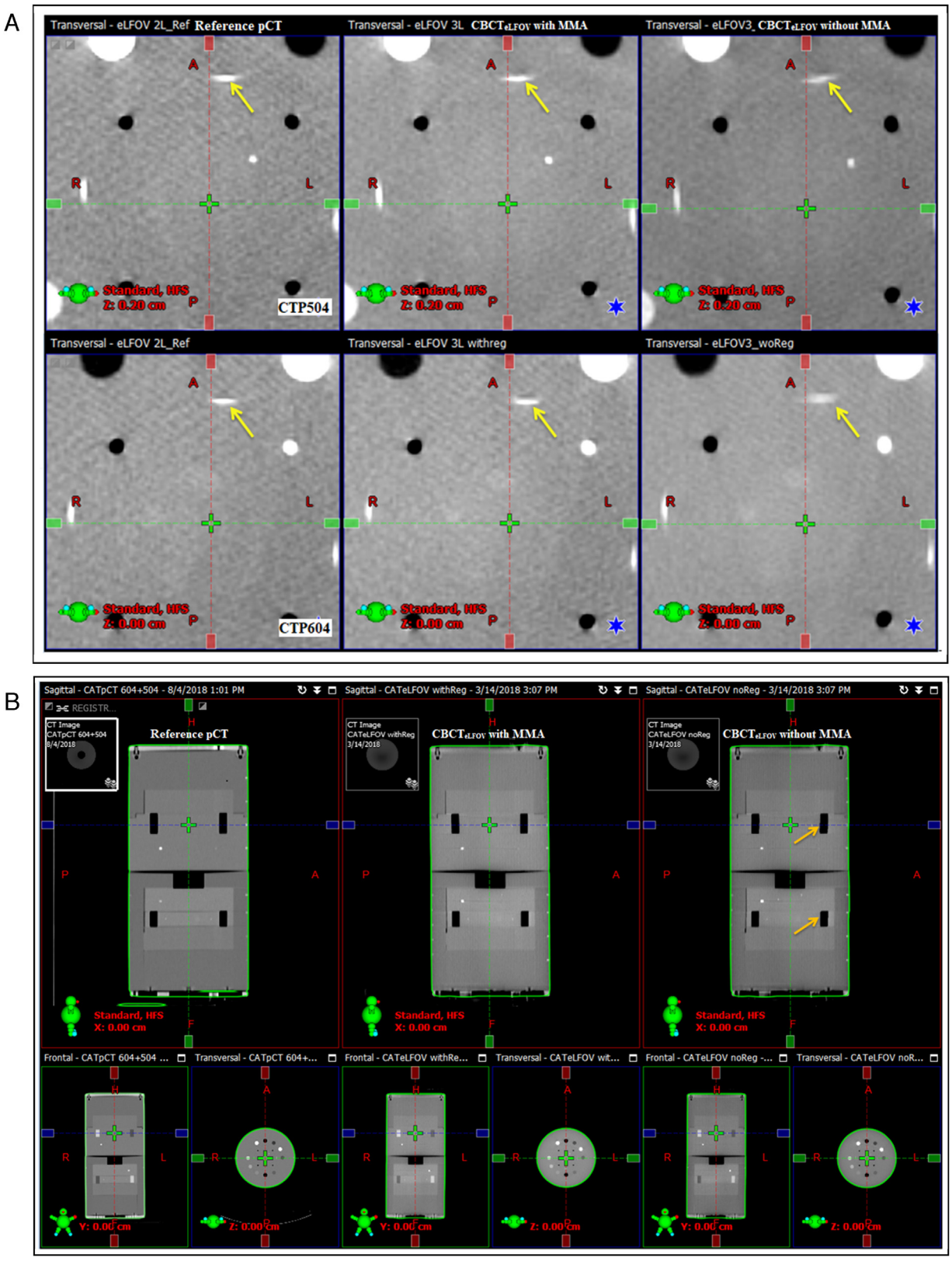

Fig. 4. (a) The fused central slices of the overlapping regions occurred at slice geometry test modules of Catphan-504 (Top) and Catphan-604 (bottom), respectively, with and without MMA (arrow marks indicate the ramp alignment). (b) The pCT and multi-scan $CBCT_{eLFOV}$ image sets (with and without MMA) of combined Catphan phantoms (arrow marks indicate minor mismatch in the $CBCT_{eLFOV}$ in the absence of MMA).

distal end of) the target (with increasing distance from the isocentre). Hence, when large narrow volumetric modulated arcs are used in the treatment plans, as in the case of CSI, such small rotations should be corrected. The actual CSI treatment workflow simulated and reported using an anthropomorphic phantom was found to be consistent with that of the patient study showing that the typical

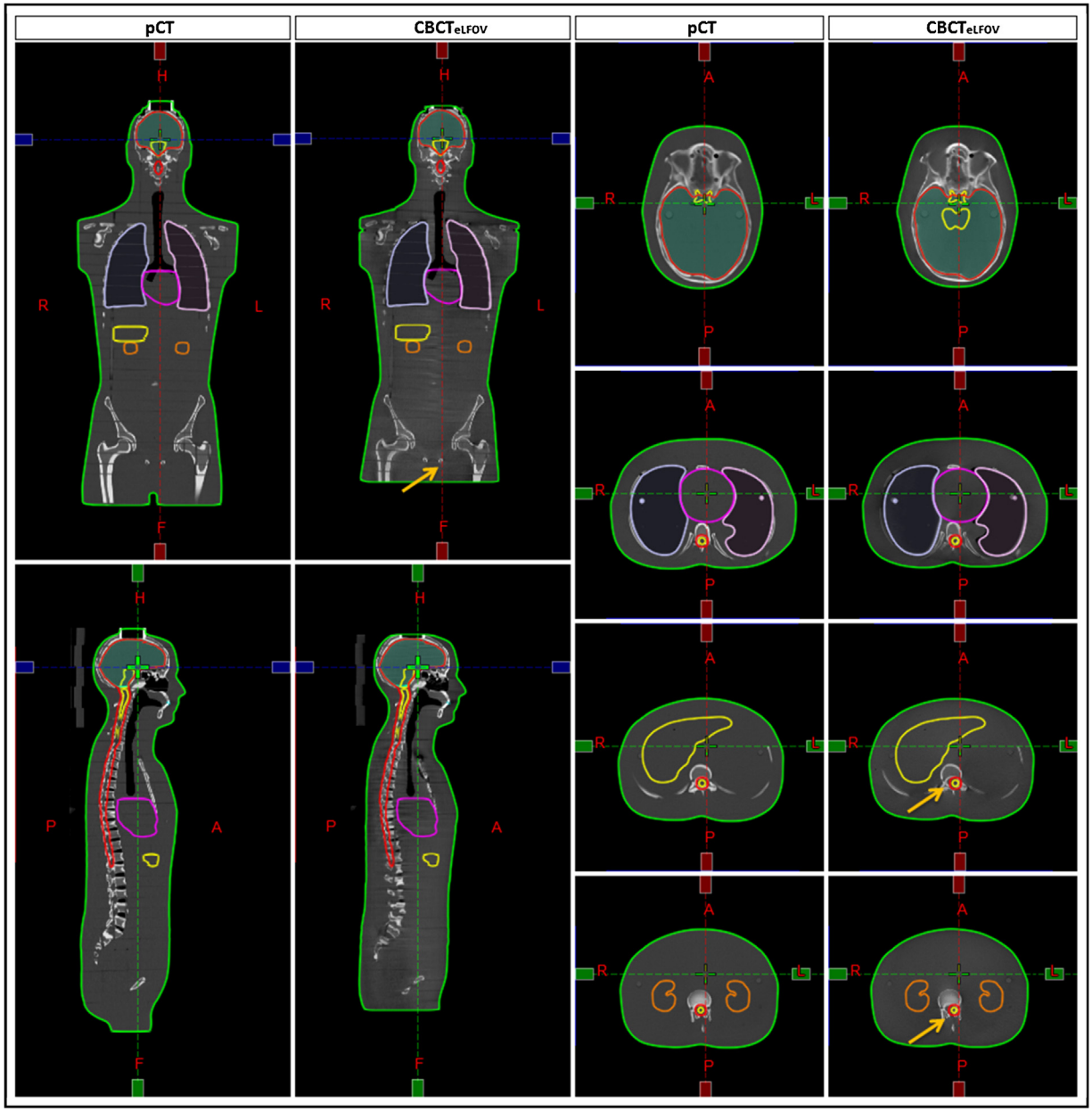

Fig. 5. Illustration of minor rotational shift in treatment setup during online localization with anthropomorphic phantom (arrow marks show the spatial displacements).

single CBCT guidance is not clinically adequate for CSI treatment with VMAT.

Translational table shift or beam centre co-ordinates of the cranial and spinal arcs reported in our study were found to be similar to that reported by Madon et al.[27] Due to non-rigid anatomical transformations, the $CMS_{x,y,z}$ and DSC_{vol} evaluations between pCT and $CBCT_{eLFOV}$ showed relatively inferior results for patients as compared to the same with anthropomorphic phantom (refer Table 3). The calculated dose on the $CBCT_{eLFOV}$ image set, when compared with pCT based treatment plans, was found to have a large deviation for both the anthropomorphic phantom and the patient study. Nevertheless, identical dosimetric results were obtained when the initial pCT was deformed to $CBCT_{eLFOV}$, thereby validating the potential use of the $CBCT_{eLFOV}$ for adaptive dosimetric evaluation. Although E2E dosimetric evaluation of treatment plans of patient paradigms can demonstrate the likelihood of under-dosing the target volume, it is unknown whether these dosimetric deviations would transform into reduced rate of tumor control.

VMAT has improved the quality of CSI treatments in terms of target dose conformity and homogeneity, sparing of OARs and healthy tissues as well as management of abutting treatment portal junctions.[32] However, ensuring precision in its delivery (i.e. to reduce the risk of radiation induced myelitis or local tumor failure due to over- or under-dosage) is still a challenge that needs special attention to realize the treatment objectives.[6] Although re-alignment of daily setup was rarely needed for CSI treatment with Vac-Lok and thermoplastic mask immobilization (33)[33], it is essential to localize the entire CSA with on-table treatment position. Since conventional localization protocols enable local matching of anatomical regions about the beam centre, they do not predict possible uncertainties beyond the actual longi-FOV (~16 cm), especially at the treatment beam boundaries and abutting regions. Target localization and treatment setup accuracy for CSI have not been extensively evaluated and presented in literature. To our knowledge, this is the first study on the entire CSA localization and adaptive evaluation with CBCT;

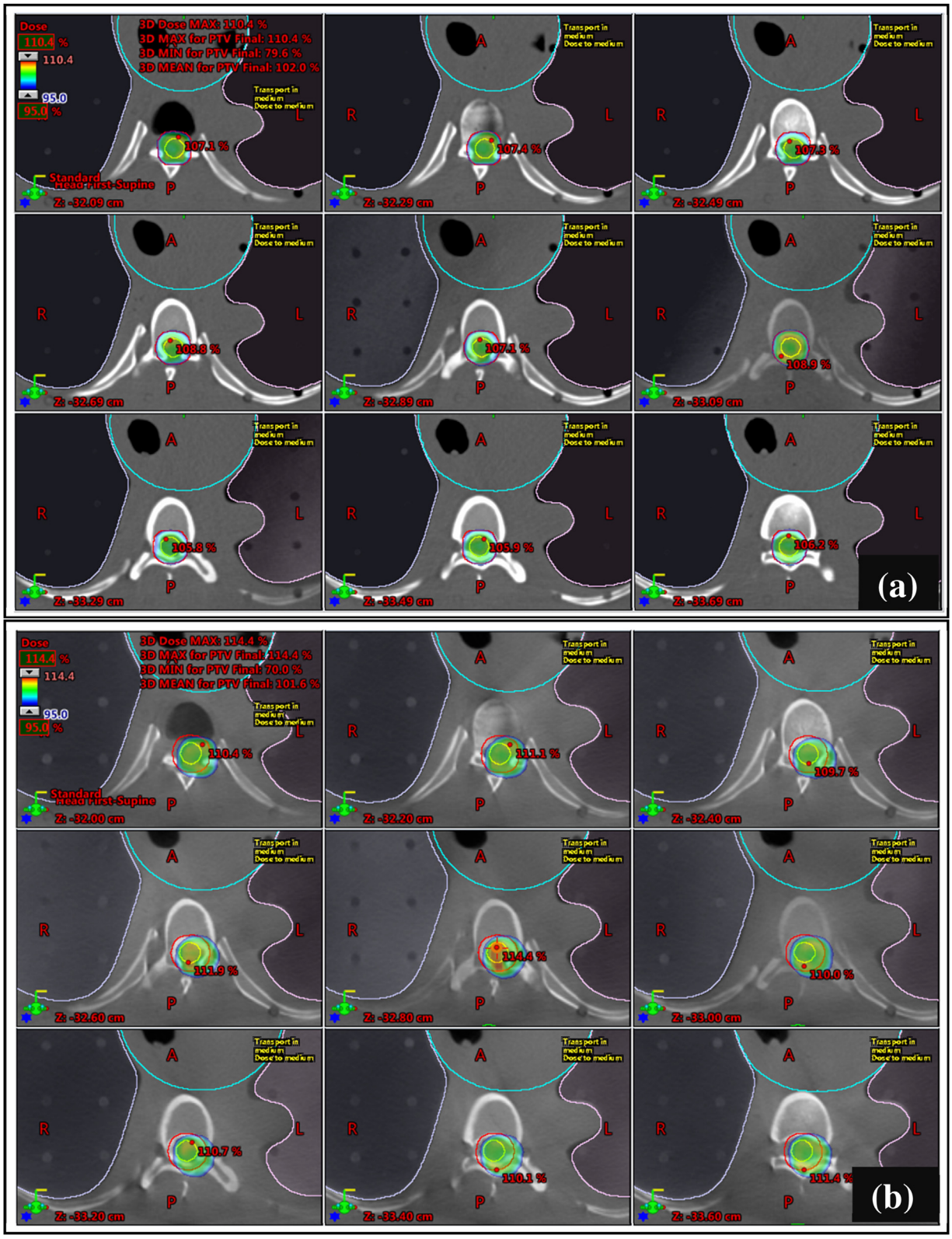

Fig. 6. The deviation from original dose distribution at the spinal PTV regions across the field boundaries of the anthropomorphic phantom. (a) pCT and (b) $CBCT_{eLFOV}$.

therefore, detailed comparison with other studies could not be made.

Olch et al. reported the importance of proactive error mitigation during complex CSI treatments with VMAT, consisting of 2 or more isocenters with dosimetrically homogenized overlapping junctions.[19] Their study revealed the need for additional QA steps to mitigate the potential for error arising out of CSI treatment and recommended such efforts for other clinics for improved clinical workflow. The riskiest step in the treatment process that could result in spinal cord overdose is reported as misapplication of image

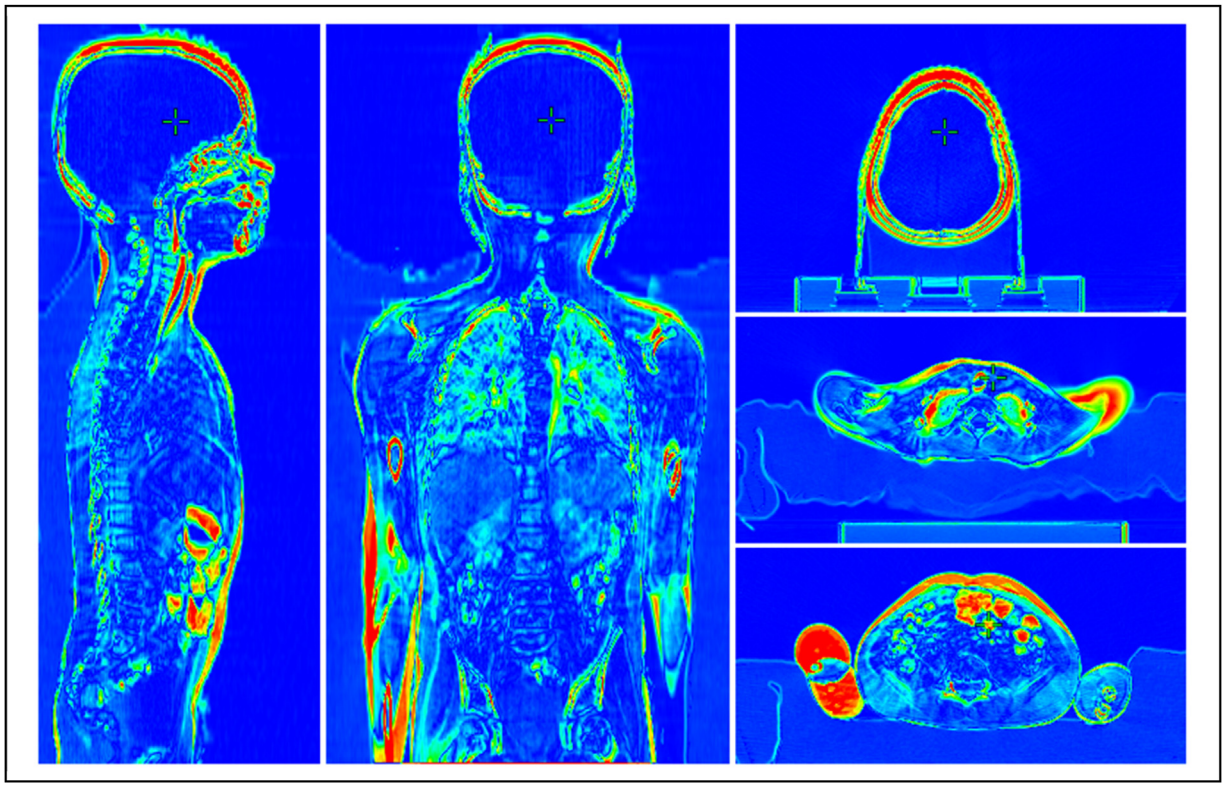

Fig. 7. The difference in rigid registration between pCT and $CBCT_{eLFOV}$ (acquired on-table treatment position) of one patient with irreproducible hand position.

guidance.[19] Until now, no report/protocol has been published to facilitate comprehensive improvement of the CSI treatment process.

While our study substantiates the importance of the proposed protocol, it is not practically feasible to perform routine $CBCT_{eLFOV}$ in a busy clinic. Therefore, implementation of similar methodology based on 2D/2D global matching using fused planar radiographs and reference DRR registrations in regular frequency can be considered as a suitable alternative. Moreover, the time required for pre-treatment daily image guidance was significantly decreased for planar radiograph-DRR registration compared to pCT-CBCT registration.[33]

While the absence of contrast administration in CBCT result in reduced spatial information, the presence of excessive scattered photons reaching the detector panel (in broad cone beam geometry) can lead to a non-uniform biasing of HU values known as cupping artifacts in $CBCT_{eLFOV}$ images.[20,21,34] Therefore, it may not be viable to update the inter-fraction anatomical changes on the $CBCT_{eLFOV}$ as accurately as on the pCT without appropriate image processing and HU corrections methods. Since the dose calculation accuracy is mainly dependent on the HU values (and not on the spatial information), the deformed pCT was primarily added to validate the practical usefulness of HU-corrected $CBCT_{eLFOV}$ for adaptive dose calculation.[30] The deformed pCT approach appears to be particularly advantageous over the conventional repeat CT and $CBCT_{eLFOV}$ based adaptive evaluation methods when updating the temporal non-rigid changes observed in each treatment fraction. However, the clinical aspect of deformation accuracy will require further investigation with specific metrics to analyze the same.

The dosimetric deviations from the original plans reported in our study were primarily a combined effect of irreproducible treatment setup and change in patient anatomy. With the two clinical cases, it is impractical to isolate the dosimetric outcome only due to variations in setup geometry (which are more appropriate in CSI treatment) than anatomical deformation. However, further investigations with large patient populations relating dosimetric outcomes with common inter-fraction uncertainties in the course of the CSI would be required to demonstrate the clinical significance of our protocol.

At present, in our clinic, we perform on-table $CBCT_{eLFOV}$ based dosimetric review of all patients with considerable change in body mass, irreproducible treatment setups and identified by the consulting physician. Inclusion of anatomical structure association (or dissociations) metrics during online pCT-CBCT registration protocols in addition to the isocentre shift co-ordinates may be considered in the future for more realistic evaluation of inter-fraction uncertainties. Based on our finding, we recommend $CBCT_{eLFOV}$ based localization of the entire CSA and adaptive dosimetric evaluation to be routinely performed during the course of treatment. Furthermore, everyday planar radiograph-DRR registration with similar strategy can also be followed to ensure high precision in treatment delivery.

5. Conclusion

The proposed protocol serves as a guide for precise localization of the entire craniospinal axis that is clinically essential to address the uncertainties beyond the actual longi-FOV of standard CBCT. The $CBCT_{eLFOV}$ based adaptive dosimetric verification will help in ensuring adequate dose to the complex craniospinal targets. Further investigation tracking the entire course of CSI treatment with a larger sample size may provide more details in terms of dosimetric outcome and their clinical significance. The standardization of online imaging protocols and incorporation of accumulated imaging dose in the therapeutic plan can facilitate frequent $CBCT_{eLFOV}$ image guided CSI. This protocol can also be adapted for the accurate treatment of complex treatment techniques such as total marrow irradiation and total lymphoid irradiation.

Financial disclosure

This project was funded in part by Atomic Energy Regulatory Board (AERB), Mumbai, India.

Conflict of interest

None declared.

Acknowledgements

The authors would like to thank Mr Joel T and Mr Nirmal Rajkumar, Radiation Therapy Technologists, Department of Radiation Oncology, Christian Medical College, Vellore, for their help in phantom simulation and planning CT acquisition. The research work presented in this manuscript is a part of the Ph. thesis submitted to the Tamil Nadu Dr. M.G.R. Medical University.

References

1. Wang K, Meng H, Chen J, Zhang W, Feng Y. Plan quality and robustness in field junction region for craniospinal irradiation with VMAT. *Phys Med*. 2018;48:21–26.
2. Leal T, Chang JE, Mehta M, Robins HI. Leptomeningeal metastasis: challenges in diagnosis and treatment. *Curr Cancer Ther Rev*. 2011;7(4):319–327.
3. Phillips C, Willis D, Cramb J, Chicas-Angulo F, Sexton M. A modified technique for craniospinal irradiation in children designed to reduce acute and late radiation toxicity. *Australas Radiol*. 2004;48(2):188–194.
4. Hadley A, Ding GX. A single-gradient junction technique to replace multiple-junction shifts for craniospinal irradiation treatment. *Med Dosim*. 2014;39(4):314–319.
5. Scott RL. An overview of craniospinal axis fields and field matching. *Med Dosim Off J Am Assoc Med Dosim*. 2013;38(4):424–429.
6. Fogliata A, Bergström S, Cafaro I, et al. Cranio-spinal irradiation with volumetric modulated arc therapy: a multi-institutional treatment experience. *Radiother Oncol*. 2011;99(1):79–85.
7. Lee YK, Brooks CJ, Bedford JL, Warrington AP, Saran FH. Development and evaluation of multiple isocentric volumetric modulated arc therapy technique for craniospinal axis radiotherapy planning. *Int J Radiat Oncol*. 2012;82(2):1006–1012.
8. Otto K. Volumetric modulated arc therapy: IMRT in a single gantry arc: single arc radiation therapy. *Med Phys*. 2007;35(1):310–317.
9. Cao F, Ramaseshan R, Corns R, et al. A three-isocenter jagged-junction IMRT approach for craniospinal irradiation without beam edge matching for field junctions. *Int J Radiat Oncol*. 2012;84(3):648–654.
10. Panandiker AP, Ning H, Likhacheva A, et al. Craniospinal irradiation with spinal IMRT to improve target homogeneity. *Int J Radiat Oncol*. 2007;68(5):1402–1409.
11. Fathy S, Alalawi T, Al-Dhaibani N. Treatment planning evaluation of volumetric modulated arc therapy (VMAT) for craniospinal irradiation (CSI). *Int J Radiat Oncol Biol Phys*. 2017;99(2):E658.
12. Chen J, Chen C, Atwood TF, et al. Volumetric modulated arc therapy planning method for supine craniospinal irradiation. *J Radiat Oncol*. 2012;1(3):291–297.
13. Paraskevopoulou C, Synodinou M, Kollias G, et al. Cranio-spinal irradiation of pediatric patients using volumetric modulated ARC therapy. *Phys Med*. 2016;32:272.
14. Wang Z, Jiang W, Feng Y, et al. A simple approach of three-isocenter IMRT planning for craniospinal irradiation. *Radiat Oncol*. 2013;8(1):217.
15. Seppälä J, Kulmala J, Lindholm P, Minn H. A method to improve target dose homogeneity of craniospinal irradiation using dynamic split field IMRT. *Radiother Oncol*. 2010;96(2):209–215.
16. Myers P, Stathakis S, Gutiérrez AN, Esquivel C, Mavroidis P, Papanikolaou N. Dosimetric comparison of craniospinal Axis irradiation (CSI) treatments using helical tomotherapy, SmartarcTM, and 3D conventional radiation therapy. *Int J Med Phys Clin Eng Radiat Oncol*. 2013;02:30.
17. Lee YK, Kim AT, Zhao P, Karotki A. Practical dose delivery verification of craniospinal IMRT. *J Appl Clin Med Phys*. 2015;16(6):76–83.
18. Ling CC, Yorke E, Fuks Z. From IMRT to IGRT: frontierland or neverland? *Radiother Oncol*. 2006;78(2):119–122.
19. Olch AJ, Bowlin KD, Chlebik A, Wong K. Process and failure mode assessment for VMAT craniospinal irradiation. *Int J Radiat Oncol*. 2015;93(3):E498.
20. Bandurska-Luque A, Piotrowski T, Skrobała A, Ryczkowski A, Adamska K, Kaźmierska J. Prospective study on dosimetric comparison of helical tomotherapy and 3DCRT for craniospinal irradiation - A single institution experience. *Rep Pract Oncol Radiother*. 2015;20(2):145–152.
21. Sun Y, Liu G, Chen W, et al. Dosimetric comparisons of craniospinal axis irradiation using helical tomotherapy, volume-modulated arc therapy and intensity-modulated radiotherapy for medulloblastoma. *Transl Cancer Res*. 2019;8(1):191–202.
22. Verbakel WFAR, Cuijpers JP, Hoffmans D, Bieker M, Slotman BJ, Senan S. Volumetric intensity-modulated arc therapy vs. conventional IMRT in head-and-neck cancer: a comparative planning and dosimetric study. *Int J Radiat Oncol*. 2009;74(1):252–259. Available from: http://www.sciencedirect.com/science/article/pii/S0360301609000303.
23. Zong-wen S, Shuang-yan Y, Feng-lei D, et al. Radiotherapy for adult medulloblastoma: evaluation of helical tomotherapy, volumetric intensity modulated arc therapy, and three-dimensional conformal radiotherapy and the results of helical tomotherapy therapy. *Biomed Res Int*. 2018. Available from: https://www.hindawi.com/journals/bmri/2018/9153496/.
24. Bichay T, Cao D, Orton CG. Helical tomotherapy will ultimately replace linear accelerator based IMRT as the best way to deliver conformal radiotherapy: point/counterpoint. *Med Phys*. 2008;35(5):1625–1628. Available from: http://doi.wiley.com/10.1118/1.2885365.
25. Myers P, Stathakis S, Mavroidis P, Esquivel C, Papanikolaou N. Evaluation of localization errors for craniospinal axis irradiation delivery using volume modulated arc therapy and proposal of a technique to minimize such errors. *Radiother Oncol*. 2013;108(1):107–113. Available from: https://linkinghub.elsevier.com/retrieve/pii/S0167814013002466.
26. Strojnik A, Méndez I, Peterlin P. Reducing the dosimetric impact of positional errors in field junctions for craniospinal irradiation using VMAT. *Rep Pract Oncol Radiother*. 2016;21(3):232–239. Available from: https://www.ncbi.nlm.nih.gov/pmc/articles/PMC5002014/.
27. Madon E, Sardo A, Sirgiovanni S, et al. EP-1795: evaluation of CBCT protocols in craniospinal RT for pediatric medulloblastoma: a preliminary study. *Radiother Oncol*. 2016;119:S841.
28. Rong Y, Smilowitz J, Tewatia D, Tomé WA, Paliwal B. Dose calculation on KV cone beam CT images: an investigation of the Hu-density conversion stability and dose accuracy using the site-specific calibration. *Med Dosim*. 2010;35(3):195–207. Available from: http://www.sciencedirect.com/science/article/pii/S0958394709000521.
29. Rafic KM, Amalan S, Timothy Peace BS, Ravindran BP. Extended localization and adaptive dose calculation using HU corrected cone beam CT: Phantom study. *Rep Pract Oncol Radiother*. 2018;23(2):126–135.
30. Rafic KM, Timothy Peace SB, Manu M, Arvind S, Ravindran BP. A rationale for cone beam CT with extended longitudinal field-of-view in image guided adaptive radiotherapy. *Phys Med*. 2019;62:129–139.
31. McMahon RL, Larrier NA, Wu QJ. An image-guided technique for planning and verification of supine craniospinal irradiation. *J Appl Clin Med Phys*. 2011;12(2):184–190.
32. Teoh M, Clark CH, Wood K, Whitaker S, Nisbet A. Volumetric modulated arc therapy: a review of current literature and clinical use in practice. *Br J Radiol*. 2011;84(1007):967–996.
33. Pfeffer RM, Tsvang L, Alezra D, Symon Z. Craniospinal irradiation (CSI) with VMAT: implementation and individual quality assurance. *Int J Radiat Oncol*. 2012;84(3):S281.
34. Altunbas MC, Shaw CC, Chen L, et al. A post-reconstruction method to correct cupping artifacts in cone beam breast computed tomography. *Med Phys*. 2007;34(7):3109–3118.